Editors' Suggestion | Featured in Physics

Quincke Oscillations of Colloids at Planar Electrodes

Zhengyan Zhang,[1] Hang Yuan,[2] Yong Dou,[1] Monica Olvera de la Cruz,[3,2,*] and Kyle J. M. Bishop[1,†]
[1]Department of Chemical Engineering, Columbia University, New York, New York 10027, USA
[2]Applied Physics Program, Northwestern University, Evanston, Illinois 60208, USA
[3]Department of Materials Science and Engineering, Northwestern University, Evanston, Illinois 60208, USA

(Received 12 February 2021; revised 25 April 2021; accepted 17 May 2021; published 23 June 2021)

Dielectric particles in weakly conducting fluids rotate spontaneously when subject to strong electric fields. Such Quincke rotation near a plane electrode leads to particle translation that enables physical models of active matter. In this Letter, we show that Quincke rollers can also exhibit oscillatory dynamics, whereby particles move back and forth about a fixed location. We explain how oscillations arise for micron-scale particles commensurate with the thickness of a field-induced boundary layer in the nonpolar electrolyte. This work enables the design of colloidal oscillators.

DOI: 10.1103/PhysRevLett.126.258001

Solid particles in weakly conducting fluids have long been known to rotate spontaneously when subject to static electric fields above a critical magnitude [1]. So-called Quincke rotation derives from the field-induced charging of the particle surface to create an unstable dipolar contribution that relaxes by mechanical rotation in the external field. Rotation near a solid boundary enables particle propulsion underlying recent experimental models of active matter [2–4]. The Quincke instability is well described by the Taylor-Melcher leaky dielectric model, which treats the fluid as a homogeneous Ohmic conductor containing no free charge [5,6]. For nonpolar electrolytes [7–9] subject to strong fields, the validity of this assumption requires the rapid generation and recombination of charge carriers within the fluid. To maintain an electric current, carriers must be generated within fluid volumes of finite thickness near system boundaries. Within such boundary layers, the assumption of the leaky dielectric model breaks down, and new types of electrohydrodynamic phenomena can arise.

For a symmetric binary electrolyte, the boundary layer thickness can be approximated as $\ell' = e\mu E_e/k_r n_o$, where e, μ, and n_o are the charge, mobility, and density of carriers, respectively; E_e is the external field strength; and k_r is a rate constant for ion recombination. Carriers are removed from the boundary region at a rate equal to the flux $e\mu n_o E_e$. At steady state, this flux is balanced by carrier generation within the boundary layer, which occurs at a rate equal to that of carrier recombination in the bulk $k_r n_o^2$. For nonpolar solutions of sodium dioctyl sulfosuccinate (AOT) surfactant commonly used in the study of Quincke rollers, external fields are expected to generate boundary layers as large as 10 μm—comparable to the size of colloidal particles.

In this Letter, we investigate the dynamics of particles within such field-induced boundary layers and observe oscillatory motions that are not predicted by the leaky dielectric model. Our experiments are based on polystyrene spheres dispersed in AOT-hexadecane solutions above a planar electrode. The application of an electric field above a critical magnitude causes the particles to roll steadily across the electrode surface [2]. On further increasing the field strength, however, the particles begin to oscillate back and forth with an amplitude comparable to their diameter. This behavior was briefly noted in previous work [10]; however, the mechanism underlying particle oscillations was not investigated or explained.

Owing to their small size, the oscillations cannot be attributed to inertial effects. Moreover, simulations based on the leaky dielectric model are unable to reproduce the observed oscillations—even when accounting for the proximal electrode. By relaxing model assumptions to account for the finite rates of ion formation and recombination, we show how Quincke oscillations can arise for particles comparable in size to the boundary layer thickness. Oscillations derive from new couplings among the charge moments on the particle surface introduced by asymmetries in the rates of charging within the boundary layer. Consistent with this mechanism, we demonstrate that oscillations are not observed for larger particles that extend beyond the boundary layer or for particles moving within the bulk electrolyte. Together, these results enable the design of colloidal oscillators and highlight the significance of electric boundary layers on the active motions of particles and their ensembles.

In our experiments, polystyrene spheres are dispersed at low volume fraction in hexadecane solutions of AOT surfactant. The suspension is sandwiched between parallel electrodes, where the particles sediment under gravity to the lower boundary [Fig. 1(a)]. On application of an external field E_e, the particles move on the electrode surface as captured by high-speed video microscopy. Depending on the strength of the applied field, we observe

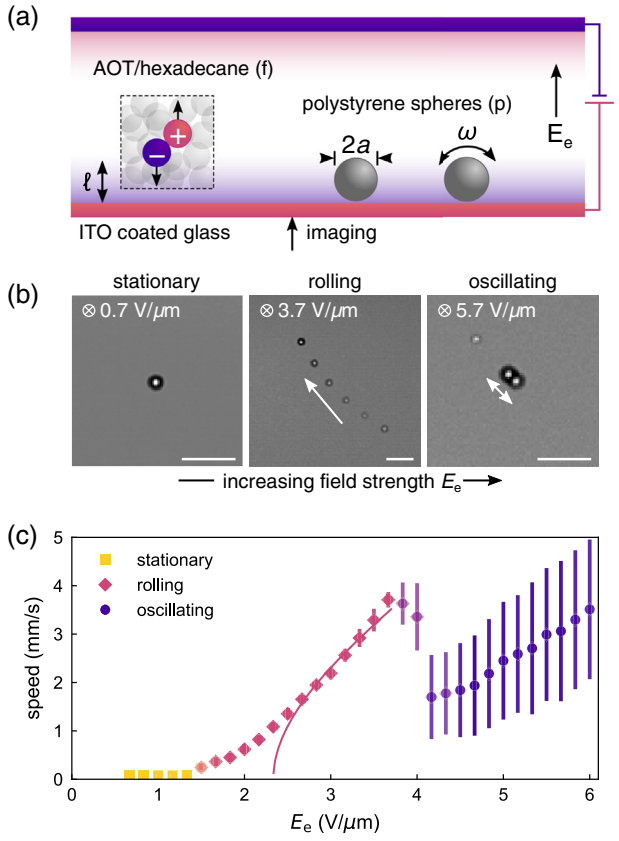

FIG. 1. (a) Schematic illustration of the experimental setup. The inset shows the ionization of AOT micelles, which is balanced by recombination in the bulk and by field-induced migration in boundary regions of thickness ℓ. (b) Time-lapse microscopy images showing the three observed particle behaviors: stationary, rolling, and oscillating. Here, the particle radius is $a = 5$ μm, the AOT concentration is [AOT] = 150 mM, and the electrode separation is $L = 150$ μm. Scale bars are 40 μm. See also Supplementary Material [11], Video 1. (c) Time-averaged particle speed vs external field strength E_e. For each 20-ms trajectory, we compute the mean and standard deviation of the particle speed. Markers denote the median of these mean speeds for ca. 1000 trajectories; error bars denote the median of the corresponding standard deviations. The plotted data are colored based on probability assignments of the Bayesian classifier. The solid curve is a fit of the form $U = (\kappa a/\tau_{\mathrm{mw}})[(E_e/E_o)^2 - 1]^{1/2}$ with $\kappa = 0.40$ and $E_o = 2.3$ V/μm; the Maxwell-Wagner time is $\tau_{\mathrm{mw}} = 0.70$ ms from independent conductivity measurements (Supplemental Material [11], Sec. 1). Note that the fitted value of the field strength E_o differs from that predicted by Eq. (1) for an unbounded sphere, $E_c = 0.91$ V/μm.

three types of particle motion termed stationary, rolling, and oscillating [Figs. 1(b) and 1(c)].

For external fields weaker than a critical value, particles remain motionless [Fig. 1(b), left]. Above this value, particles roll along the electrode in random directions perpendicular to the applied field with a constant speed [Fig 1(b), middle]. Further increasing the field, we observe a second transition whereby particles cease to roll and instead oscillate back and forth [Fig. 1(b), right]. The time-averaged particle speed increases with field strength before slowing abruptly at the onset of oscillations [Fig. 1(c), markers]. Accompanying this transition from rolling to oscillating, temporal variations in particle speed increase in magnitude from zero to a finite value [Fig. 1(c), error bars]. In addition to these descriptive statistics, we use Bayesian model selection [12,13] to classify each particle trajectory based on competing models for stationary, rolling, and oscillating dynamics [Fig. 1(c), colors; see Supplemental Material [11], Sec. 2].

The observed transition from stationary to rolling agrees qualitatively with predictions of the leaky dielectric model for a spherical particle immersed in an unbounded fluid with respective permittivities ε_p, ε_f and conductivities σ_p, σ_f. The model predicts that the stationary solution becomes unstable when the external field strength exceeds the critical value [14–16]

$$E_c = \sqrt{\frac{2\eta}{\varepsilon_f \tau_{\mathrm{mw}}(\varepsilon_{\mathrm{cm}} - \sigma_{\mathrm{cm}})}}, \tag{1}$$

where η is the fluid viscosity, $\tau_{\mathrm{mw}} = (\varepsilon_p + 2\varepsilon_f)/(\sigma_p + 2\sigma_f)$ is the Maxwell-Wagner time, and $x_{\mathrm{cm}} = (x_p - x_f)/(x_p + 2x_f)$ for $x = \varepsilon, \sigma$ are the Claussius-Mossotti factors characterizing the high- and low-frequency polarizability of the sphere, respectively. Above this field, the angular velocity and thereby the rolling speed U increase with increasing field strength as $U = (\kappa a/\tau_{\mathrm{mw}})[(E_e/E_c)^2 - 1]^{1/2}$, where $\kappa \leq 1$ is a dimensionless coefficient characterizing the strength of rotation-translation coupling [Fig. 1(c), solid curve]. Consistent with this model, the critical field strength is independent of particle radius a but increases with increasing AOT concentration, which increases the conductivity of the fluid (Supplemental Material [11], Secs. 3.1 and 3.2).

Near the transition from rolling to oscillating, particles exhibit a mixture of intermediate behaviors such as rolling in a common direction with a time-periodic speed and rolling with aperiodic reversals in direction (Supplemental Material [11], Sec. 3. 3). Similar behaviors attributed to inertial effects were reported for larger spheres ($a = 50$ μm) under stronger confinement ($L/a \approx 4$) [17]. Here, we neglect this transition region and focus instead on the previously undescribed phenomenon of back-and-forth oscillations.

Oscillatory dynamics are reliably observed for strong fields, $E_e/E_c > 3$, when the ratio between the particle radius and the boundary layer thickness is of order unity, $a/\ell \sim 1$ (Fig. 2). In estimating this length scale, $\ell = e\mu E_e/k_r n_o$, we approximate the mobility of AOT micelles as $\mu = (6\pi\eta a_h)^{-1}$ where $a_h = 1.7$ nm is the reported hydrodynamic radius [9]. We further assume that the rate constant for neutralizing collisions among charged

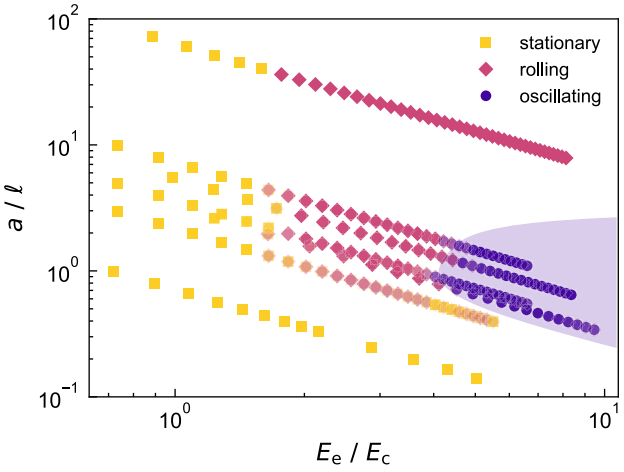

FIG. 2. Phase diagram showing the observed dynamics as a function of two dimensionless parameters: a/ℓ, the ratio of the particle radius and the boundary layer thickness; E_e/E_c, the ratio of the external field strength and the critical field of Eq. (1). Plotted data correspond to experiments on five different particle sizes $a = 0.5, 1.5, 2.5, 5, 25\ \mu$m (for $[\mathrm{AOT}] = 150$ mM) and three different AOT concentrations $[\mathrm{AOT}] = 50$, 100, 150 mM (for $a = 5\ \mu$m). Markers are colored based on probability assignments of the Bayesian classifier (Supplemental Material [11], Sec. 2).

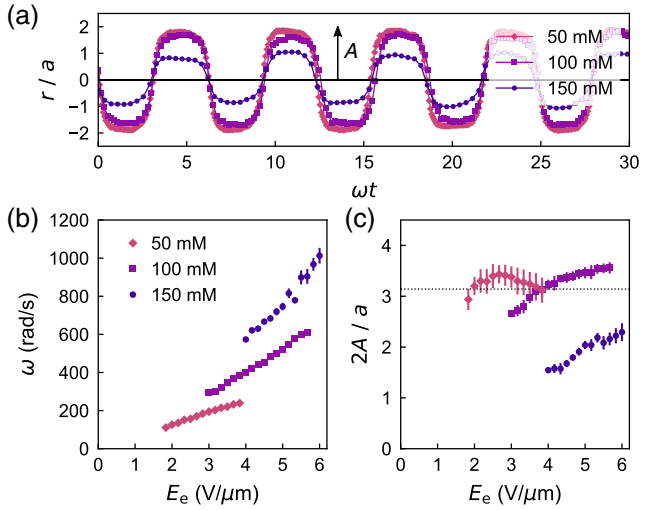

FIG. 3. (a) Particle position r vs time t for PS spheres (radius $a = 5\ \mu$m) in different AOT-hexadecane solutions. The applied field is $E_e/E_c = 5.4$, which corresponds to $E_e = 2.2$, 3.7, and 4.8 V/μm for $[\mathrm{AOT}] = 50$, 100, and 150 mM, respectively. (b) Oscillation frequency ω vs external field strength E_e for different AOT concentrations. Markers denote the mean frequencies within populations of particle trajectories of equal duration; error bars denote standard deviations of these populations. (c) Peak-to-peak oscillation amplitude $2A$ vs external field strength E_e for the three AOT concentrations in (b). Markers denote the mean frequencies; error bars denote standard deviations.

micelles is diffusion limited such that $k_r = 2e^2\mu/\varepsilon_f$ [6,18]. Finally, we estimate the concentration of charged micelles from the measured conductivity as $n_o = \sigma_f/2e^2\mu$ (Supplemental Material [11], Sec. 1). The resulting boundary layer thickness ℓ varies from 1 to 20 μm depending on the AOT concentration and the external field strength. Notably, large particles ($a/\ell \gg 1$) that extend beyond the boundary region do not oscillate but rather roll at even the highest fields investigated (Fig. 2). Small particles ($a/\ell \ll 1$) do not move at all; their otherwise Brownian motion is arrested upon application of the field (Supplemental Material [11], Sec. 3.4).

The frequency of particle oscillations ω is comparable to the dipolar relaxation rate τ_{mw}^{-1} and increases with increasing field strength [Figs. 3(a) and 3(b)]. Experiments at different AOT concentrations suggest that the oscillation frequency is well approximated as $\omega \approx 0.09\tau_{\mathrm{mw}}^{-1}E_e/E_c$ (Supplemental Material [11], Sec. 3.5). This form is identical to that of the rolling frequency predicted by the leaky dielectric model, suggesting that the oscillation frequency is set by a similar balance of particle rotation and charge accumulation at the particle surface.

The peak-to-peak amplitude of the oscillating particle position is approximately $2A \approx \pi a$ [Fig. 3(c)]. This observed quantity is linearly related to the angle $2A/\kappa a$ by which the particle rotates during each half of the oscillation cycle. If one assumes frictional rolling with $\kappa = 1$, the observed amplitude would imply a rotation of ca. 180°. By contrast, the assumption of hydrodynamic rolling with a thin lubricating film [19,20] requires that $\kappa \leq 1/4$ and implies a rotation of at least two revolutions per half cycle. Below, we present a model for particle oscillations that favors the former interpretation based on frictional rolling.

Owing to the small size of the particles, the observed oscillations cannot be attributed to inertial effects. The Reynolds number for particle oscillations is much less than unity, $\mathrm{Re} = \rho\omega a^2/\eta \sim 10^{-3}$, where ρ is the fluid density. The hydrodynamic resistance to motion is therefore proportional to the particle velocity. Moreover, particle inertia is also negligible as evidenced by the small Stokes number, $\mathrm{St} = \rho_p a^2/15\eta\tau_{\mathrm{mw}} \sim 10^{-4}$, where ρ_p is the density of the particle. With finite particle inertia, Quincke dynamics of a sphere in an unbounded fluid is mathematically identical to the Lorenz system [21] and to the Malkus water wheel [22], which are known to exhibit oscillatory and chaotic dynamics [23]. In the absence of inertial effects, however, only the stationary and rolling solutions are permitted by the leaky dielectric model in an unbounded fluid.

Control experiments on particles within the bulk fluid suggest that oscillatory dynamics occur only near the electrode surface. We use a standing acoustic field to levitate particles at the midplane between two planar electrodes [24] and observe their motion upon application of the electric field (Supplemental Material [11], Sec. 4 and

Video 2). In the absence of the acoustic field, the application of a strong electric field drives the particles to oscillate at the electrode surface. Such oscillations are not observed when the same field is applied to particles levitating at the midplane of the chamber. Instead, particles in the bulk fluid exhibit steady rotation consistent with predictions of the leaky dielectric model.

To understand why particles of intermediate size oscillate near the electrode (see Fig. 2), we first consider the transport of charged AOT micelles around a stationary sphere near a plane boundary [Figs. 4(a) and 4(b)]. The electric field and the carrier densities are modeled using the Poisson-Nernst-Planck (PNP) equations modified to describe the generation and recombination of charged micelles within the electrolyte [6,25] (Supplemental Material [11], Sec. 5). At steady state, the solution is characterized by three length scales: the particle radius a, the Debye length $\lambda_D = (\varepsilon_f k_B T/2e^2 n_o)^{1/2}$, and the boundary layer thickness ℓ associated with carrier recombination. We focus our analysis on the limit of strong fields relevant to our experiments, for which $E_e \gg k_B T/e\ell$ or, equivalently, $\ell \gg \lambda_D$. At the anode (cathode), we assume that the injection of positive (negative) charge carriers is negligible compared to their formation within the electric boundary layer [26]. Under these conditions, the behavior of large spheres ($a \gg \ell$) is well described by the leaky dielectric model. Charge accumulates at the particle surface as to redirect the electric field and the associated electric current around the particle [Fig. 4(a)]. The Quincke instability is caused by the relaxation of this dipolar charge distribution via particle rotation.

For small spheres ($a \ll \ell$), however, the accumulation of charge at the particle surface is mitigated by the diffusive leaking of charge carriers around the sides [Fig. 4(b)]. The comparatively little charge that accumulates does not significantly alter the electric field. Without a sufficiently large dipole moment directed antiparallel to the external field, there can be no Quincke rotation for these small particles (cf. Fig. 2). Moreover, such particles are characterized by a net charge that contributes additional electrostatic forces directed to the nearby electrode. The attraction of small particles to the electrode surface helps to explain the field-induced arrest of their Brownian motion.

For particles of intermediate size ($a \sim \ell$), the observed oscillations are explained by asymmetries in the rates of charging between the top and bottom of the particle. Within the confined region separating the particle and the electrode, ionic currents are limited by the finite rate of ion formation in the fluid. Within such a region of thickness δ, the ion current does not exceed $k_r n_o^2 \delta$, which is less than the ion current in the bulk, $e\mu n_o E_e$, provided that $\delta < \ell$ (Supplemental Material [11], Sec. 5). As a result, the bottom half of the particle surface charges more slowly than the top half. This asymmetric charging can be incorporated qualitatively into the leaky dielectric model

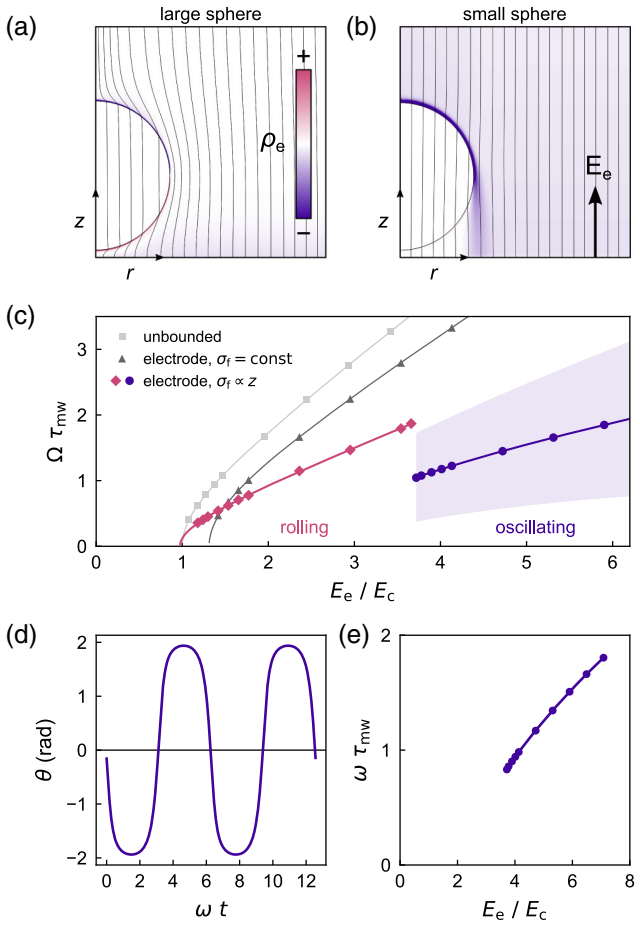

FIG. 4. (a),(b) Simulated electric field around a stationary sphere in a model electrolyte above a plane electrode; color map shows the charge density [11]. The radii of the large (a) and small (b) spheres are $a/\ell = 3.5$ and $a/\ell = 0.14$, respectively. Other parameters include the Debye length $\lambda_D/\ell = 0.028$, the surface separation $\delta/a = 0.1$, the particle permittivity $\varepsilon_p/\varepsilon_f = 1.2$, and the recombination rate constant $k_r\varepsilon_f/e^2\mu = 2$. (c) Time-averaged angular speed Ω scaled by τ_{mw}^{-1} vs external field strength E_e scaled by E_c for three variations of the leaky dielectric model: an unbounded sphere, a sphere at a plane electrode with constant fluid conductivity, and a sphere at an electrode with a conductivity gradient. The particle permittivity is $\varepsilon_p/\varepsilon_f = 1.5$; the surface separation is $\delta/a = 0.1$; the conductivity gradient is $\sigma_f/(2a+\delta)$; the resistance coefficient is $R/8\pi\eta a^3 = 1.45$. The shaded region denotes one standard deviation about the average speed. (d) Angular position θ vs oscillation phase ωt for $E_e = 5.3E_c$. (e) Oscillation frequency ω scaled by τ_{mw}^{-1} vs external field strength E_e scaled by E_c.

by introducing a position-dependent fluid conductivity that increases linearly with distance z from the electrode surface. This approximate treatment avoids the computationally challenging task of solving the time-dependent PNP equations governing the formation, transport, and recombination of charged micelles. With the addition of the conductivity gradient, numerical simulations of the leaky

dielectric model effectively reproduce the particle oscillations observed in experiment [Fig. 4(c), pink diamonds and blue circles].

In the model, we consider a dielectric sphere of radius a immersed in a conductive fluid at a distance δ from a plane electrode (Supplemental Material [11], Sec. 6). Application of an external field E_e drives the accumulation of charge at the particle-fluid interface; the effects of free charge within the electrolyte are neglected. The fluid conductivity is assumed to vary with distance z from the electrode as $\sigma_f z/(2a+\delta)$, approaching the bulk value σ_f at the top of the particle. The angular velocity of the particle (parallel to the plane) is linearly related to the electric torque as $\Omega = T/R$, where $R = 8\pi\eta a^3 f(\delta/a)$ is the relevant resistance coefficient. With these assumptions, the particle dynamics agree qualitatively with the experimental observations [cf. Figs. 1(c) and 4(c)]. At sufficiently high field strengths—here, greater than 3.7 times the critical field E_c for an unbounded sphere—the particle oscillates back and forth with a peak-to-peak amplitude of ca. 200° [Fig. 4(d)]. The oscillation frequency ω increases in proportion to the external field strength E_e [Fig. 4(e)].

Physically, particle oscillations combine the basic elements of the traditional Quincke mechanism—namely, charge accumulation and mechanical relaxation—with new couplings among the charge moments introduced by the conductivity gradient. For a sphere in an unbounded fluid of constant conductivity, the dynamics of Quincke rotation can be described in terms of the particle's dipole moment, which evolves independently from the other moments [14,15]. Within a conductivity gradient, however, the disturbance field produced by one moment leads to currents that alter the others. Inspection of the transient charge moments for an oscillating sphere reveal a quadrupole moment that is approximately constant in the particle reference frame (see Supplementary Material [11], Sec. 6.3 and Fig. S15). The disturbance field produced by this quadrupole contributes to the charging of the dipole moment as to reverse the direction of rotation, thereby enabling back-and-forth oscillations. Similar oscillatory dynamics are observed in a closely related mechanical model, a modified Malkus water wheel [22,23] with overdamped dynamics and position-dependent leakage (Supplemental Material [11], Sec. 7 and Video 3).

To conclude, asymmetric charging within electric boundary layers results in Quincke oscillations of colloids in the absence of inertial effects or electrohydrodynamic flows. Additional experiments on particles of different shapes suggest that these oscillations can be achieved for any dielectric particle of suitable size (Supplemental Material [11], Sec. 8 and Video 4). This mechanism may therefore provide a useful experimental model for active matter [27] comprised of many self-oscillating units, where particle interactions—neglected herein—mediate their collective dynamics. More generally, Quincke oscillations illustrate the potential importance of field-induced boundary layers within nonpolar fluids. Even away from electrode surfaces, such boundary layers are expected to influence the dynamics of micron-scale Quincke swimmers [28–30].

This work was supported as part of the Center for Bio-Inspired Energy Science, an Energy Frontier Research Center funded by the U.S. Department of Energy, Office of Science, Basic Energy Sciences under Award DE-SC0000989.

*m-olvera@northwestern.edu
†kyle.bishop@columbia.edu

[1] G. Quincke, Ueber rotationen im constanten electrischen felde, Ann. Phys. (N.Y.) **295**, 417 (1896).
[2] A. Bricard, J.-B. Caussin, N. Desreumaux, O. Dauchot, and D. Bartolo, Emergence of macroscopic directed motion in populations of motile colloids, Nature (London) **503**, 95 (2013).
[3] A. Bricard, J.-B. Caussin, D. Das, C. Savoie, V. Chikkadi, K. Shitara, O. Chepizhko, F. Peruani, D. Saintillan, and D. Bartolo, Emergent vortices in populations of colloidal rollers, Nat. Commun. **6**, 7470 (2015).
[4] B. Zhang, A. Sokolov, and A. Snezhko, Reconfigurable emergent patterns in active chiral fluids, Nat. Commun. **11**, 4401 (2020).
[5] J. R. Melcher and G. I. Taylor, Electrohydrodynamics: A review of the role of interfacial shear stresses, Annu. Rev. Fluid Mech. **1**, 111 (1969).
[6] D. A. Saville, Electrohydrodynamics: The Taylor-Melcher leaky dielectric model, Annu. Rev. Fluid Mech. **29**, 27 (1997).
[7] D. C. Prieve, B. A. Yezer, A. S. Khair, P. J. Sides, and J. W. Schneider, Formation of charge carriers in liquids, Adv. Colloid Interface Sci. **244**, 21 (2017).
[8] S. K. Sainis, J. W. Merrill, and E. R. Dufresne, Electrostatic interactions of colloidal particles at vanishing ionic strength, Langmuir **24**, 13334 (2008).
[9] M. Kotlarchyk, J. S. Huang, and S. H. Chen, Structure of AOT reversed micelles determined by small-angle neutron scattering, J. Phys. Chem. **89**, 4382 (1985).
[10] N. Desreumaux, Emulsions microfluidiques et rouleurs colloïdaux: Effets collectifs en matiére molle forcée hors-équilibre, thesis, Université Pierre et Marie Curie—Paris VI, 2015, p. 99.
[11] See Supplemental Material at http://link.aps.org/supplemental/10.1103/PhysRevLett.126.258001 for (1) electrical characterization of the AOT-hexadecane electrolyte, (2) details on data collection and analysis, (3) additional experimental data, (4) description of acoustic levitation experiments, (5) analysis of a model electrolyte in 1d, (6) numerical solution of the leaky dielectric model, (7) mechanical analogy of an oscillating waterwheel, and (8) experimental results for cylindrical particles.
[12] D. Sivia and J. Skilling, *Data Analysis: A Bayesian Tutorial* (Oxford University Press, Oxford, 2006).
[13] C. K. Williams and C. E. Rasmussen, *Gaussian Processes for Machine Learning* (MIT Press Cambridge, MA, 2006).

[14] T. B. Jones, Quincke rotation of spheres, IEEE Trans. Ind. Appl. **IA-20**, 845 (1984).
[15] D. Das and D. Saintillan, Electrohydrodynamic interaction of spherical particles under Quincke rotation, Phys. Rev. E **87**, 043014 (2013).
[16] Y. Hu, P. M. Vlahovska, and M. J. Miksis, Colloidal particle electrorotation in a nonuniform electric field, Phys. Rev. E **97**, 013111 (2018).
[17] G. E. Pradillo, H. Karani, and P. M. Vlahovska, Quincke rotor dynamics in confinement: Rolling and hovering, Soft Matter **15**, 6564 (2019).
[18] P. Debye, Reaction Rates in Ionic Solutions, Trans. Electrochem. Soc. **82**, 265 (1942).
[19] S. Kim and S. J. Karrila, *Microhydrodynamics* (Dover, New York, 2005).
[20] A. J. Goldman, R. G. Cox, and H. Brenner, Slow viscous motion of a sphere parallel to a plane wall–i motion through a quiescent fluid, Chem. Eng. Sci. **22**, 637 (1967).
[21] E. N. Lorenz, Deterministic nonperiodic flow, J. Atmos. Sci. **20**, 130 (1963).
[22] M. Kolár and G. Gumbs, Theory for the experimental observation of chaos in a rotating waterwheel, Phys. Rev. A **45**, 626 (1992).
[23] F. Peters, L. Lobry, and E. Lemaire, Experimental observation of Lorenz chaos in the Quincke rotor dynamics, Chaos **15**, 013102 (2005).
[24] S. Sabrina, M. Tasinkevych, S. Ahmed, A. M. Brooks, M. Olvera de la Cruz, T. E. Mallouk, and K. J. M. Bishop, Shape-directed microspinners powered by ultrasound, ACS Nano **12**, 2939 (2018).
[25] F. Peters, L. Lobry, A. Khayari, and E. Lemaire, Size effect in quincke rotation: A numerical study, J. Chem. Phys. **130**, 194905 (2009).
[26] A. J. Bard, L. R. Faulkner *et al.*, *Electrochemical Methods* (John Wiley & Sons, Inc., New York, 2001), Vol. 482, pp. 94–96.
[27] M. C. Marchetti, J.-F. Joanny, S. Ramaswamy, T. B. Liverpool, J. Prost, M. Rao, and R. A. Simha, Hydrodynamics of soft active matter, Rev. Mod. Phys. **85**, 1143 (2013).
[28] D. Das and E. Lauga, Active Particles Powered by Quincke Rotation in a Bulk Fluid, Phys. Rev. Lett. **122**, 194503 (2019).
[29] L. Zhu and H. A. Stone, Propulsion driven by self-oscillation via an electrohydrodynamic instability, Phys. Rev. Fluids **4**, 061701(R) (2019).
[30] Z. M. Sherman and J. W. Swan, Spontaneous Electrokinetic Magnus Effect, Phys. Rev. Lett. **124**, 208002 (2020).